Polymer 172 (2019) 415–422

Contents lists available at ScienceDirect

Polymer

journal homepage: www.elsevier.com/locate/polymer

Poly (vinyl butyral)/Graphene oxide/poly (methylhydrosiloxane) nanocomposite coating for improved aluminum alloy anticorrosion

Guiyu Zhu[a], Xiaokun Cui[a], Yue Zhang[a,*], Shougang Chen[a,****], Mengyao Dong[b,c], Hu Liu[c], Qian Shao[d], Tao Ding[e,**], Shide Wu[f], Zhanhu Guo[b,***]

[a] School of Material Science and Engineering, Ocean University of China, Qingdao, Shandong, 266100, China
[b] Integrated Composites Laboratory (ICL), Department of Chemical & Biomolecular Engineering, University of Tennessee, Knoxville, TN, 37996, USA
[c] Key Laboratory of Materials Processing and Mold (Zhengzhou University), Ministry of Education, National Engineering Research Center for Advanced Polymer Processing Technology, Zhengzhou University, Zhengzhou, 450002, Henan, China
[d] College of Chemical and Environmental Engineering, Shandong University of Science and Technology, Qingdao, Shandong, 266590, China
[e] College of Chemistry and Chemical Engineering, Henan University, Kaifeng, 475004, China
[f] Henan Provincial Key Laboratory of Surface and Interface Science, Zhengzhou University of Light Industry, No. 136, Science Avenue, Zhengzhou, 450001, China

HIGHLIGHTS

- Poly (methylhydrosiloxane) (PMHS) has been applied as GO/PVB composite coating.
- The influence of the GO content on the corrosion resistance was studied.
- The long-term corrosion resistance of the composite coating was tested.

ARTICLE INFO

Keywords:
Poly (vinyl butyral)
Graphene oxide
Corrosion resistance

ABSTRACT

A polyvinyl butyral (PVB)/graphene oxide (GO) nanocomposite coating was prepared via spin coating method to improve the anticorrosion ability of aluminum alloy. Poly (methylhydrosiloxane) (PMHS) has been innovatively applied as anti-corrosion coatings of aluminum substrate owing to its hydrophobicity. The properties of the coating were characterized by Fourier-transform infrared spectroscopy (FT-IR), scanning electron microscope (SEM) and other methods. Meanwhile, the corrosion resistance of the coating in 3.5 wt% NaCl solution was estimated by electrochemical impedance spectroscopy (EIS) and potentiodynamic polarization. The SEM observations showed that the coating was uniformly distributed on the surface of aluminum. EIS tests showed that the coating had a remarkable anticorrosive effect on the metal surface. Compared with bare aluminum, the low frequency impedance modulus improved three orders of magnitude, reaching $10^7\ \Omega\ cm^2$. The polarization curve showed that the corrosion current density (I_{corr}) decreased more than three orders of magnitude, reaching $7.8 \times 10^{-9}\ A\ cm^{-2}$. The long-term immersion experiment indicated that the coating could effectively protect the aluminum for up to 1200 h. This study provides a facile way of using polymer nanocomposites to tackle the corrosion of aluminum alloy for industrial applications.

1. Introduction

Ocean transportation accounts for about 90% of world trade, while metals play a very important role in ocean transport. However, metals are vulnerable to corrosion in marine environment such as sea water, marine organisms, wind and waves, etc., caused enormous economic losses [1,2]. Aluminum is a metal less susceptible to corrosion because it can rapidly form an oxide film on its surface when exposed to air to passivate the aluminum substrate and slow down the occurrence of aluminum corrosion. It becomes one of the marine vessel components for a long time [3]. Regrettably, the invasive chloride ions in marine can cause the pitting of aluminum [4]. Therefore, it is particularly

* Corresponding author.
** Corresponding author.
*** Corresponding author.
**** Corresponding author.
E-mail addresses: zhangyue@ouc.edu.cn (Y. Zhang), sgchen@ouc.edu.cn (S. Chen), dingtao@henu.edu.cn (T. Ding), zguo10@utk.edu (Z. Guo).

https://doi.org/10.1016/j.polymer.2019.03.056
Received 5 February 2019; Received in revised form 18 March 2019; Accepted 24 March 2019
Available online 27 March 2019
0032-3861/

important to protect metal matrix from corrosion in the development of marine economy [5].

The addition of corrosion inhibitor, metal surface modification, coating protection and electrochemical protection have all been used to heighten the corrosion resistance of metals [6,7]. Coating protection is an effective and traditional marine anticorrosion technology [8,9]. However, most organic coatings have the disadvantages of complex processes, high cost, and environmental pollution [10]. Thus, it is important to find an environmentally friendly coating that is simple in process and non-toxic to the environment [11].

The application of polyvinyl butyral (PVB) in coating field has attracted more and more attention and research because of its excellent heat resistance, film forming, high tensile and impact resistance, etc. Meanwhile, the presence of hydroxyl groups in PVB molecules provides active sites for chemical reactions and more possibilities for the preparation of composite coatings by chemical modification. For example, Luckachan et al. [9] fabricated anti-corrosion coatings of PVB by the addition of chitosan on mild carbon steel. Chaudhry et al. [10] studied the impedance of PVB and graphene nanocomposite coatings. Zuo et al. [12] reported the application of epoxy-PVB coating on rust mild steel. The coatings also provide corrosion resistance. Mahmoudian et al. discussed the corrosion protective performance of polypyrrole (PPy) in PVB coatings on mild steel [13]. Niratiwongkorn et al. [14] also reported composite coatings combined with PVB, PPy and carbon black on steel. The results really provided evidence for the utilization of conductive fillers in anti-corrosion coatings. In this study, PVB can be completely dissolved in ethanol, only a small amount of environmental-friendly ethanol was added as solvent in the process of coating preparation, and the solvent was completely removed after the film formation without any harm to the environment.

Graphene oxide (GO) and other conducting additives for organic coatings have intrigued great interests for their wide applications including metal corrosion protection, nanocomposite coating, energy storage/conversion, and others [15–25]. Numerous oxygen functional groups in GO make it have good dispersity and reaction activity than graphene, for instance, hydroxyl, epoxy, carboxyl and ester groups [26]. In addition, the poor conductivity of GO relative to graphene decreases the electron transfer inside the coating, thus improving the corrosion resistance of the coating. Hajian et al. [27] investigated the mechanical properties of PVB/graphene composite coatings. The results proved that the mechanical properties of the coating were significantly enhanced by mixing with graphene. However, the study did not focus on the performance of coatings in the field of corrosion protection.

In this study, the corrosion resistance of PVB/GO coatings was explored. The coupling agent known as “molecular bridge” can improve the interaction between filler and polymer. Poly (methylhydrosiloxane) (PMHS) was currently used for surface modification of coatings owing to its low surface energy and hydrophobic properties [28]. In this study, PMHS was applied to the PVB anticorrosive composite coating on the surface of aluminum matrix to enhance the degree of cross-linking and improve the surface condition of the coating. The anticorrosion behaviors of the polymer nanocomposite coating were studied by the electrochemical impedance spectroscopy (EIS, three-electrode system), Tafel polarization curve and their corresponding microstructure for the freshly prepared sample and immersed sample to disclose the anticorrosion mehcanism.

2. Experiment

2.1. Materials

Graphite powder (chemically pure) and KH-560 were obtained from Sinopharm Chemical Reagent Co., Ltd. Sodium nitrate was bought from Tianjin Beilian Fine Chemicals Development Co., Ltd. Polyvinyl butyral (M.W.40000-70000) was bought from Shanghai Macklin Biochemical Co., Ltd. Poly(methyhydrosiloxane) (viscosity: 15-40 mPa s (20 °C)) was bought from Aladdin Tndustrial Corporation. None of the chemicals used in this study was further purified.

2.2. Pretreatment of samples

Aluminum alloys were cut into pieces of 10 mm × 10 mm × 3 mm size, and sanded by SiC sandpaper with different sizes to remove surface passivation layer and then polished by diamond suspension polishing fluid (W 0.5 μm) mixed in distilled water to obtain mirror-like finish. The polished aluminum alloy pieces were disposed by acetone, ethanol, and water for 5 min in turn and then slightly corroded by 2 wt% NaOH solution for 10 s, all the above steps were done in ultrasonic cleaner. Ultimately, all of the samples were dried with nitrogen and stored in a vacuum oven.

2.3. Preparation of coatings

Graphene oxide (GO) was prepared by modified hummer method. The coating systems were prepared as follows. First, GO was dispersed in ethyl alcohol absolute. After 30-min ultrasonic dispersion, the GO particles were further dispersed by the ultrasonic cell disruptor (JY 92-IIDN). Then different contents of GO suspension (0.2 wt%, 0.3 wt%, 0.4 wt%, 0.5 wt%, 0.6 wt%) were put into the prepared PVB solution and stirred for 1 h on the magnetic stirrer at room temperature. The reaction was continued for 3 h after adding 1 mL KH-560 or PMHS in order to investigate the effects of KH-560 and PMHS on the coating. Finally, the solution was coated on the aluminum alloy surface with a spin-coating method and dried for 6 h in a vacuum drying oven (DZF-6020) at 100 °C to obtain the coating. The preparation process and reaction mechanism of coating system were simply described in Fig. 1.

2.4. Characterization

Fourier transform infrared spectroscopy within a range of 4000–500 cm^{-1} was used to characterize the functional groups of GO. The surface topographies of the coatings were observed by SEM.

The corrosion properties of samples were characterized by electrochemical impedance spectroscopy (EIS, three-electrode system) and polarization curve in 3.5 wt% NaCl solution. A three-electrode system with platinum counter electrode, silver/silver chloride reference electrode and aluminum plate electrode coated with different coatings working electrode was used for electrochemical testing. The surface area of the sample was 1 cm^2, and the test process was carried out at room temperature. The frequency range of EIS test was 10^5–10^{-2} Hz and the amplitude was 10 mV. The voltage range of polarization curve was −1.4–0 V, and the scanning rate was 10 mV/s. The samples were all immersed in 3.5 wt% sodium chloride solution for 30 min in advance before test.

3. Results and discussions

3.1. FTIR and Raman spectrograms of GO

As can be seen from Fig. 2, GO has a wide and strong absorption peak at 3406 cm^{-1}, which corresponds to the O−H stretching vibration of hydroxyl groups. The absorption peaks at 1740 cm^{-1} and 1400 cm^{-1} correspond to the stretching vibration of C═O and the deformation vibration of O−H in carboxyl groups, respectively. The absorption peaks at 1260 cm^{-1}, 1100 cm^{-1}, and 1630 cm^{-1} proved the existence of epoxy groups, ether bond and unsaturated C═C double bond [15,21]. In summary, a high degree of oxidation was obtained from GO, and many oxygen-containing functional groups, including hydroxyl, carboxyl, epoxy group and ether bond, etc. appeared and provided more possibilities for the subsequent chemical reaction [29].

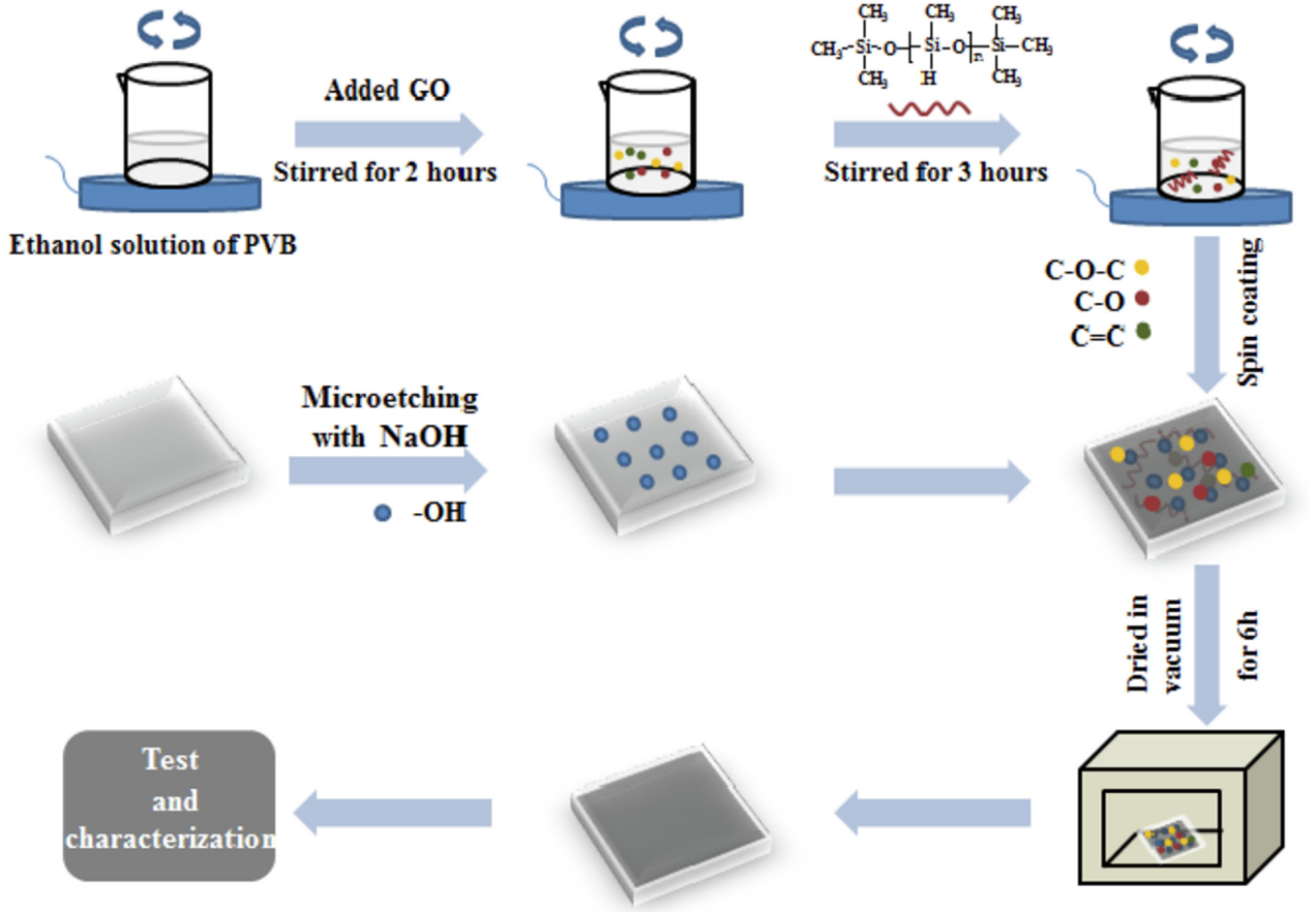

Fig. 1. Sketch map of preparation process and reaction mechanism of the coating.

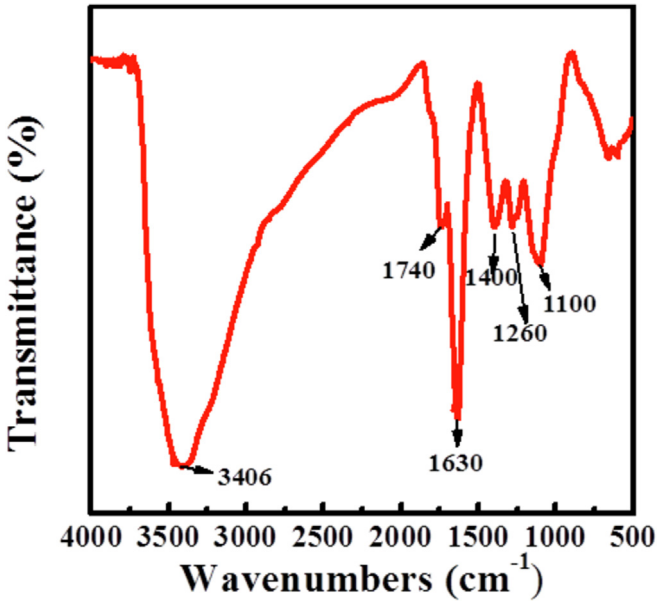

Fig. 2. FT-IR spectrum of GO.

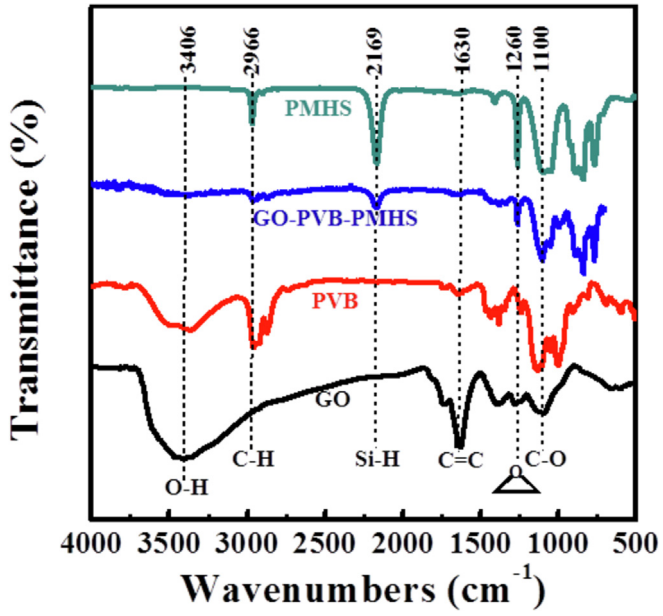

Fig. 3. FT-IR spectra of coating.

3.2. FTIR spectrogram of the composite coating

The infrared absorption peaks of GO, PVB, PMHS and the composite coating were all presented in Fig. 3. The main absorption peaks of the samples have been marked in the diagram. As can be seen from Fig. 3, a lot of oxygen-containing functional groups like hydroxyl (3406 cm^{-1}), epoxy group (1260 cm^{-1}) and ether bond (1100 cm^{-1}), etc. exist in the molecular structure of GO and PVB, and endow excellent reactivity

between them [9]. The absorption peaks at 2966 cm^{-1}, 2169 cm^{-1} and 1630 cm^{-1} are due to the stretching vibration of methyl ($-CH_3$), silicon hydrogen bond (Si—H) and carbon-carbon double bond (C=C), separately [28,30].

Many methyl groups in the molecular structure of PMHS resulted in its hydrophobicity and the high chemical activities of Si—H bonds enabled it undergo numerous chemical reactions. Through analysis, the weakened absorption peaks at 2966 cm^{-1} ($-CH_3$) and 2169 cm^{-1} (Si—H) indicated the occurrence of a forceful interaction among various parts of reagents. The disappearance of the absorption peaks of GO/PVB/PMHS coating at 3406 cm^{-1} (—OH) and 1630 cm^{-1} (C=C) and the attenuation of absorption peaks at 1260 cm^{-1} ( ) and 1100 cm^{-1} (C—O) indicated the reduction of oxygen functional groups and the addition reaction of C=C.

Besides, the absorption bands at 1260 cm^{-1} could also be interpreted as the bending vibration of $Si—CH_3$. Furthermore, the silicon-hydrogen bonds in the PMHS had a complex addition reaction with the C=C bonds in GO to form a large number of silicon-carbon bonds, the attenuation of the absorption peak at 2169 cm^{-1} (Si—H) and the absorption peak of $Si—CH_3$ at 1260 cm^{-1} proved this fact further. In addition, the silicon-hydrogen bonds combined with the hydroxyl groups in PVB during the preparation of the coating, resulted in a good dispersion of GO and complex cross-linking structure of the coating [31,32]. All of the above evidences interpreted the successful cross-linking and preparation of GO/PVB/PMHS coating.

3.3. Microstructure of the composite coatings

Fig. 4 shows the SEM morphology of uncoated and coated samples to describe the dispersion of the coating on aluminum surface. It can be seen from Fig. 4(a) that there were some scratches and spot defects on the surface of the sample due to the process of mechanical polishing and slight corrosion with NaOH solution. From Fig. 4(b), **(c)** and **(d)**, the surface of coating was smooth without obvious defects, the uniform and dense microstructure of the coating can effectively prevent the corrosive ions from entering. On the other hand, the addition of granular GO influenced the uniformity of the coating as shown in Fig. 4(c), and made the coating distributed unevenly on the sample surface, forming a cotton flocculent structure. The GO/PVB/PMHS coated sample

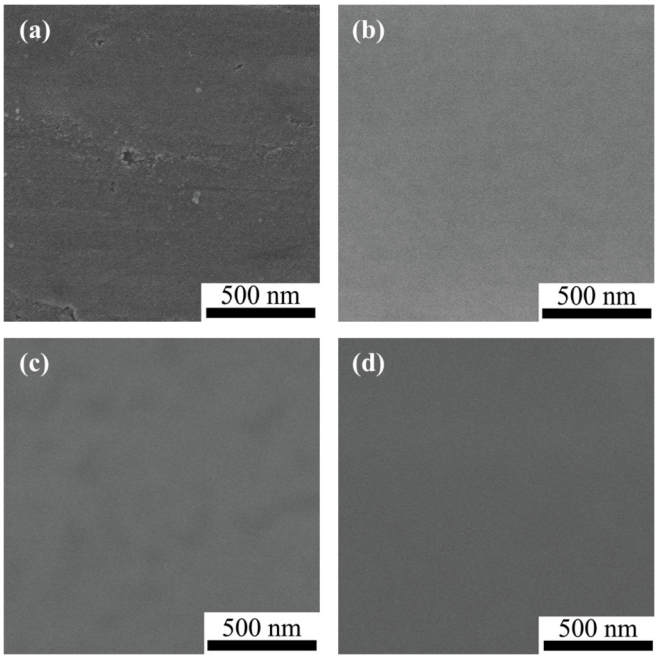

Fig. 4. SEM images of **(a)** uncoated sample, **(b)** pure PVB, **(c)** GO/PVB, **(d)** GO/PVB/PMHS coated sample.

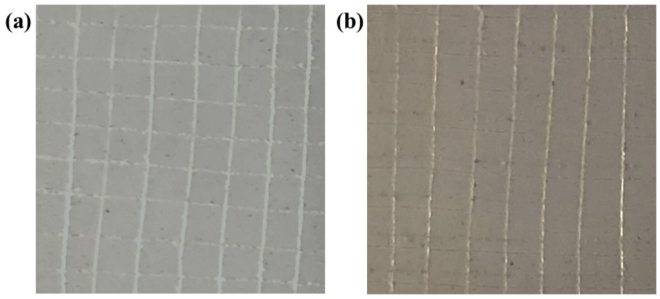

Fig. 5. Adhesion test diagram of coating. (a) before and (b) after testing.

(Fig. 4(d)) was very smooth compared with GO/PVB coatings of Fig. 4(c). It was obvious that the addition of PMHS improved the dispersion of GO in the PVB system, and the coating was uniformly distributed on the surface of the sample. A well-proportioned and compact film was formed. The well-dispersed GO filler made the diffusion channel of corrosive ions more complicated and prolonged the path of corrosive ions to the surface of aluminum accordingly. Thus, the metal substrate could be well protected.

The cross square on the surface of the coating was scratched with the blade, and cleaned carefully with a brush, stuck the tape firmly on the sample for a moment and then took it off. The adhesion of the coatings can be judged by the number of dropped lattices. Compared the pictures before and after the adhesion test in Fig. 5, no obvious exfoliation phenomenon was observed in the coating after testing, which indicated that the coating had a strong adhesion. It was tightly bonded with the metal matrix. The excellent adhesion comes from two aspects. On one hand, it is closely related to the role of PMHS. A large number of intermolecular crosslinks and reorganizations made the coating form a complex network structure, the good bonding was formed with the aluminum alloy matrix, too. On the other hand, the micro-corrosion process by NaOH on the surface of aluminum sheet also enhanced the bonding ability between the coating and the substrate. The strong adhesion guarantees the long-term protection of the coatings on aluminum alloy matrix.

3.4. Hydrophobic properties of the composite coatings

Fig. 6(a) shows the water contact angles of different coating systems. From the results, it obviously revealed that the contact angle of coating surface without coupling agent was 81°, which indicated the hydrophilic properties of PVB. The hydrophilic properties made other corrosion ions such as water molecules gather on the surface of the coating and entered the metal through the diffusion channel so as to accelerate the corrosion of metal. The hydrophilicity of the coating was not changed by adding KH-560 silane coupling agent. However, with the addition of PMHS, the contact angle raised to 107°, which changed the coating surface from hydrophilic to hydrophobic.

Fig. 6(b) shows the laser confocal microscope image of GO/PVB/PMHS coating. Different colors represent different relative heights of the coating as shown by the length scale on the right. It was clearly seen that the surface of the coating showed uneven topography with many hill-like protuberances due to the existence of fillers and the marginal was significantly higher than the middle part owing to the particularity of spin-coating process. From another point of view, the addition of PMHS made GO fillers dispersed uniformly without obvious agglomeration. The roughness of the coating surface after fitting calculation was 400 nm. Since the circumference of the coating was higher than the intermediate position, the actual roughness value should be slightly lower than the calculated value. According to other literature data [33], this value indicated that the coating surface was relatively rough. As we all know, the surface with low surface energy and high roughness was more hydrophobic [34]. The low surface energy and rough surface

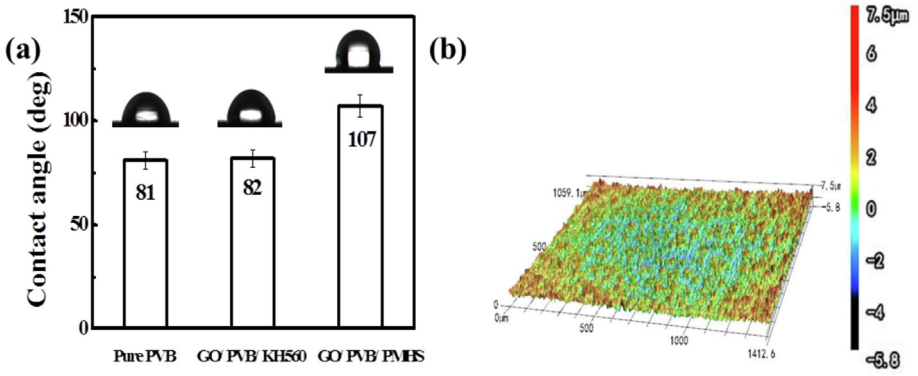

Fig. 6. (a) Contact angles of different coating systems. **(b)** 3D laser microscope of GO/PVB/PMHS coating.

structure of PMHS had a great significance to the anticorrosive property of the coating. The hydrophobic surface was not conducive to the adsorption of water molecules and other corrosive ions, so it can provide initial protection for metals to reduce the possibility of ions invading metal substrates through coating [21]. The construction of hydrophobic surface and anticorrosion components provide a dual protection for aluminum.

3.5. Corrosion resistance of coatings

3.5.1. EIS results

Fig. 7 reveals the relationship between impedance modulus, phase angle and frequency of different coating systems. The impedance value in the low frequency region has an important significance for the corrosion resistance of the coating. A higher low frequency impedance modulus represents a better corrosion resistance of the coating [35]. As shown in Fig. 7(a), the impedance of samples with different coatings in the low frequency significantly increased by several orders of magnitude compared to the uncoated sample. From Fig. 7(b), it was worthy to note that the impedance modulus of GO/PVB/PMHS system was more than three orders of magnitude and reached a maximum value of $10^7\ \Omega\,cm^2$ while the content of GO was 0.4 wt%. The low-frequency impedance modulus was obviously improved by one order of magnitude compared to the previously published data [18].

For bare aluminum, only one high phase angle peak was observed in the intermediate frequency region from Fig. 7(a), which might be explained by the overlap of two peaks, corresponding to the alumina and corrosion processes on the metal surface [36]. However, there was a broad phase angle peak in a large frequency region of GO/PVB/PMHS coating systems. It showed that the barrier ability of GO/PVB/PMHS coating systems to corrosive medium was stronger, and the metal matrix was protected from corrosion ions to some extent.

In Fig. 8(a), the capacitive resistance arc shapes of different systems were various. This shows the equivalent circuits and the corrosion resistance mechanisms of different systems are diverse from each other. It was obvious that the capacitive reactance arc of GO/PVB/PMHS coating system was much larger than that of other systems, and there were two capacitive reactance arcs, corresponding to two different time constants. The capacitive reactance arc of the high frequency area can be corresponded to the coating resistance and the coating capacitance, and the capacitance reactance in the low frequency area corresponded to the solution resistance and the charge transfer resistance. A larger capacitive reactance arc indicates a better corrosion resistance of the coating [37]. Meanwhile, Fig. 8(b) shows that the capacitive reactance arc was much larger than other contents when the content of GO was 0.4 wt%, indicating the optimum anticorrosive property of the coating.

The experimental data was fitted and appropriate equivalent circuit was selected using ZSimDemo software in order to explore the anticorrosive mechanism of GO/PVB/PMHS coating system further. Table 1 shows the fitting parameters about individual coating systems. Fig. 9 shows the equivalent circuit of the anticorrosion mechanism of GO/PVB/PMHS coating system.

R_s represents the solution resistance and C_s is the capacitance between working electrodes and electrolytes. Q (constant phase element, CPE) can be considered as a special capacitor of the coating with poor surface roughness, it represents the resistance of the outer layer of the coating together with R_c (the resistance of the coating) [35]. R_{ct} is the charge transfer resistance, which is a significant parameter to

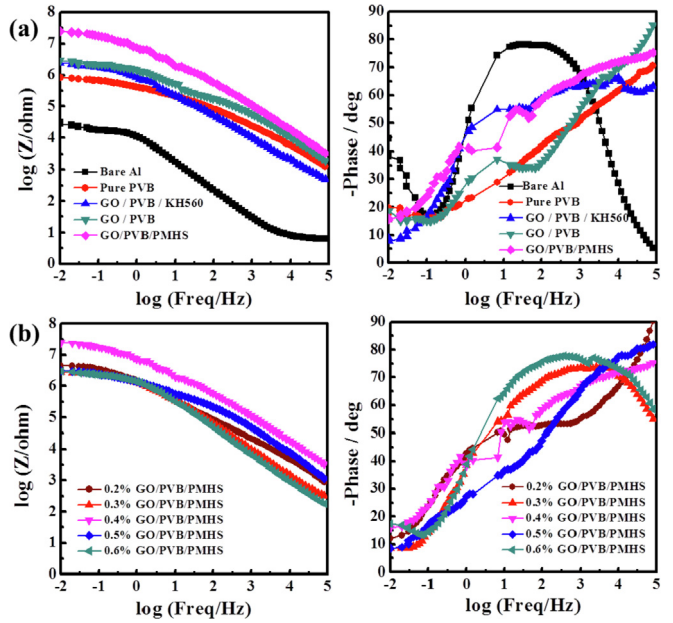

Fig. 7. Bode diagrams of **(a)** different coating systems and **(b)** GO/PVB/PMHS systems with different content of GO in 3.5 wt% NaCl solution.

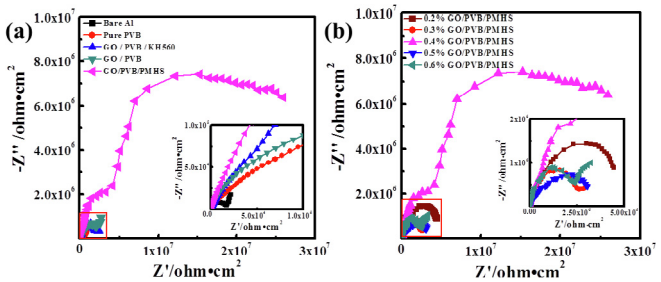

Fig. 8. Nyquist plots of(**a**) different coating systems, **(b)** GO/PVB/PMHS systems with different contents of GO in 3.5 wt% NaCl solution.

Table 1
Equivalent circuit parameters for individual coating systems.

Sample	R_s ($\Omega\cdot cm^2$)	C_s ($F\cdot cm^{-2}$)	R_{ct} ($\Omega\cdot cm^2$)	CPE (Q)		R_c ($\Omega\cdot cm^2$)	C_{dl} ($F\cdot cm^{-2}$)	R_{dl} ($\Omega\cdot cm^2$)
				$Y_0(\Omega^{-1}\cdot sncm^{-2})$	n			
0.2%GO	100	3.8×10^{-9}	5.6×10^{6}	2.3×10^{-7}	0.6	1.4×10^{4}	5.7×10^{-9}	1.6×10^{3}
0.3%GO	134.8	1.1×10^{-8}	2.9×10^{6}	1.6×10^{-7}	0.8	4.2×10^{3}	2.1×10^{-8}	1.9×10^{2}
0.4%GO	491.2	8.2×10^{-10}	3.3×10^{7}	4.0×10^{-8}	0.5	1.1×10^{4}	2.2×10^{-9}	3.4×10^{3}
0.5%GO	92.8	1.7×10^{-9}	3.6×10^{6}	2.2×10^{-7}	0.5	2.2×10^{-2}	2.5×10^{-8}	6.0×10^{4}
0.6%GO	77.5	1.2×10^{-8}	2.4×10^{6}	9.8×10^{-8}	0.8	8.5×10^{5}	8.6×10^{-6}	1.7×10^{6}

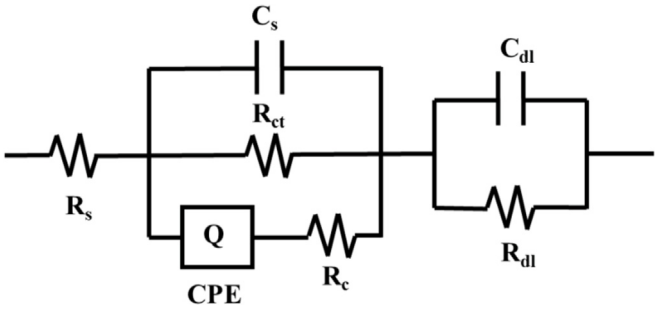

Fig. 9. Equivalent Circuit Diagram of GO/PVB/PMHS coating system.

characterize the resistance properties of the coating. Its value characterized the electron transfer across the surface. From Fig. 9, the R_{ct} of the coatings with different contents of GO all reached ten to the power of six, performed high resistance values, and therefore played better protective role on the metal matrix. The double layer capacitance (C_{dl}) and resistance (R_{dl}) represent the resistance of the inner layer of the coating [6,10,37–40].

3.5.2. Tafel polarization

Fig. 10 shows the Tafel curve of different specimen, and the homologous corrosion parameters are listed in Table 2. The E_{corr} and I_{corr} represent the corrosion potential, corrosion current density, respectively. E_{corr} characterizes the corrosion tendency of materials from the point of view of thermodynamics, meanwhile, I_{corr} characterizes the instantaneous rate of corrosion reaction of materials from the angle of kinetics [41].

According to Fig. 10(a), the E_{corr} of GO/PVB/PMHS coating system was −0.8 V, which shifted to positive direction by 64 mV compared to bare aluminum (−0.865 V). And the I_{corr} of GO/PVB/PMHS coating system was more than three orders of magnitude lower than that of bare aluminum and two orders of magnitude lower than that of coating system without PHMS coupler. This indicated that the corrosion rate of the coating was relatively slow and could protect the matrix to a large extent. In Fig. 10(b), the I_{corr} reached 7.8×10^{-9} A cm^{-2} when the content of GO in the PVB was 0.4%, the best protective effect on aluminum matrix was obtained [42]. In order to show more intuitively the protective effect of various coating systems on aluminum substrate, the

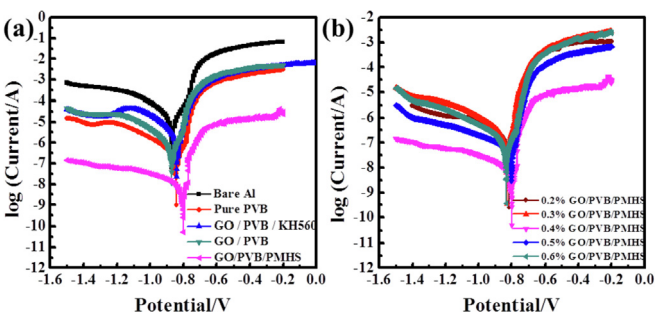

Fig. 10. Tafel curve of different coating systems.

Table 2
Polarization parameters for different coating systems.

Sample	E_{corr} (V)	I_{corr} ($A\cdot cm^{-2}$)	R_p ($\Omega\cdot cm^2$)	η
Bare	−0.86	8.5×10^{-6}	2.0×10^{3}	
PVB	−0.84	1.2×10^{-7}	9.6×10^{4}	98.5851%
GO/PVB	−0.84	1.6×10^{-6}	1.2×10^{4}	99.9393%
GO/PVB/KH560	−0.87	3.0×10^{-7}	3.9×10^{4}	99.9886%
GO/PVB/PMHS	−0.80	7.8×10^{-9}	3.2×10^{6}	99.9997%
0.2% GO	−0.81	7.6×10^{-8}	1.9×10^{5}	99.9971%
0.3% GO	−0.83	1.1×10^{-7}	1.5×10^{5}	99.9957%
0.4% GO	−0.80	7.8×10^{-9}	3.2×10^{6}	99.9997%
0.5% GO	−0.80	6.6×10^{-8}	3.1×10^{5}	99.9975%
0.6% GO	−0.83	4.2×10^{-8}	2.9×10^{5}	99.9984%

protective efficiency (η) of the coating was calculated according to formula (1):

$$\eta = \frac{I^0_{corr} - I^1_{corr}}{I^0_{corr}} \times 100\% \quad (1)$$

where I^0_{corr} and I^1_{corr} are the I_{corr} of bare aluminum and samples with different coatings, respectively [37,43].

The calculation results are listed in Table 2. From Table 2, the protective efficiency of each coating on aluminum substrate was over 99%. The optimal protection efficiency reached 99.9997% when the content of GO was 0.4 wt%.

3.6. Long-term immersion experiment

3.6.1. EIS results after long-term immersion experiment

Fig. 11 shows the electrochemical results of GO/PVB/PMHS coating after immersion in 3.5 wt% NaCl solution. After one-day immersion, the impedance ($10^7\ \Omega\ cm^2$) of the coating in low frequency decreased by one order of magnitude compared with that ($10^7\ \Omega\ cm^2$) of the coating immersed for 30 min. The impedance module of the coating decreased to above $10^5\ \Omega\ cm^2$ after 15-day immersion, and the shape of the impedance-frequency curve had been changed. In combination with the comprehensive analysis of Fig. 11(b), the phase angle-frequency curve has also changed, and two peaks appear in the curve. The results indicated that corrosion ions have invaded the surface of the coating to

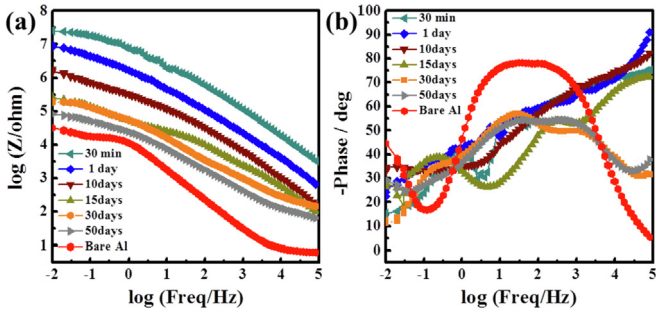

Fig. 11. Bode diagrams of GO/PVB/PMHS coating systems after long-term immersion experiment.

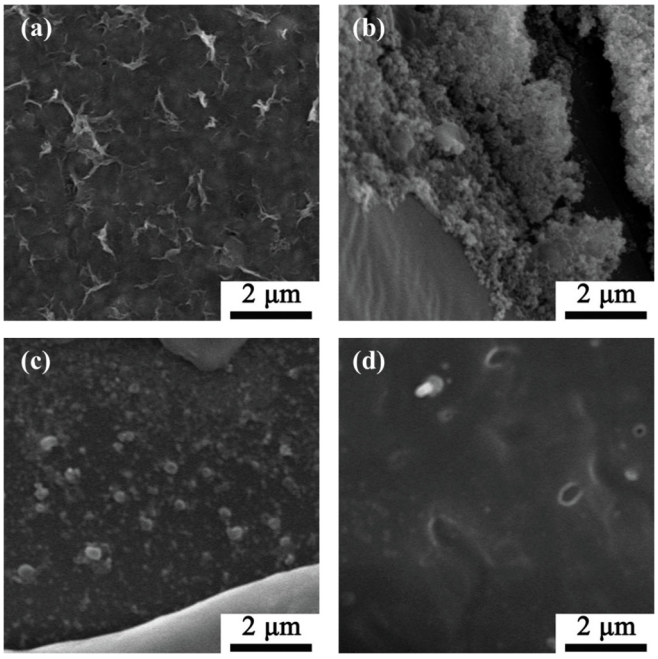

Fig. 12. SEM images of **(a)** bare aluminum, **(b)** PVB coating, **(c)** GO/PVB coating, **(d)** GO/PVB/PMHS coating after long-term immersion experiment.

corrode and the corrosion product was accumulated, transformed the protective mechanism of the coating on the metal substrate.

Moreover, after immersion for 50 days, the low frequency impedance module of the coating almost decreased to the order of magnitude close to that of the bare aluminum. Fig. 11(b) displays that the phase angle-frequency curve has changed again compared to 15-day immersion. The two peaks in the curve disappeared and a wider peak appeared in the intermediate frequency region. This may be interpreted as the corrosive ions intruded into the interior of the coating, passed through the coating, and finally reached the metal substrate, resulting in corrosion of metal and more corrosion products were accumulated on the coating surface at the same time. Therefore, it can be considered that the coating has almost lost its protective effect on the metal substrate at this time.

3.6.2. Microstructure after long-term immersion experiment

Scanning electron microscopy (SEM) was used to observe the surface state of the coating during immersion, Fig. 12 shows the SEM morphology of the coatings after immersion in 3.5 wt% NaCl solution for 30 days. For the bare aluminum, Fig. 12(a), it can be seen that there were many micron scale cracks on the surface of the sample, which divide the coating surface into scales-like lamellae. This indicates that the aluminum surface has been severe corrode.

As observed in Fig. 12(b), a large area of particles crystallized on the surface of aluminum with PVB coating and there had a broken part like a gully on the right side of the images. Due to the hydrophilicity of PVB, a large amount of solution was adsorbed on the sample surface. With the prolongation of immersion, the high concentration solution gradually crystallized on the surface of the sample. In this case, the surface of the sample has been severe corroded. As seen in Fig. 12(c), there were many punctate particles on the surface of the sample. The reason of this phenomenon may be that the present GO formed an active site for the aggregation of corrosive ions and thus the point-liked corrosion products were produced. It can be inferred that with the prolongation of immersion, the corrosion ions further eroded the metal matrix through these sites. Compared with the uniform coating before immersion, the surface of the specimen was basically intact but with a small number of pits appeared after 30-day immersion, as presented in Fig. 12(d).

At the same time, a small amount of corrosion product appeared on the surface of the coating. Judged from the area and depth of pits, the surface of the sample was slightly pitting but the coating still had the protective capability on the metal to some extent. Compared with the morphology of GO/PVB coating system, Fig. 12(c), it is difficult for the solution to adhere to the surface of the sample owing to the hydrophobic nature of PMHS, thereby greatly reduced the invasion chance of corrosion ions. It can be speculated that these pitting pits will certainly become the source of corrosion expansion in the future. The corrosion ions would drive through these pitting channels to invade the metal substrate, and caused the loss of the protective effect of the coating on aluminum surface.

4. Conclusion

A new kind of PVB nanocomposite coating was successfully prepared for anticorrosion of aluminum alloy substrate in marine environment. The added PMHS with hydrophobic properties made the hydrophobic surface of the composite coating, which was of great significance to reinforce the corrosion resistance of the coating. These results showed that the surface of the coating was uniform and compact, hydrophobic and had a strong adhesion with the metal substrate. Electrochemical measurement displayed that the GO/PVB/PMHS coating exhibited a remarkably anticorrosive effect on the metal surface. The optimum content of GO in PVB coating was 0.4 wt%. Compared with bare aluminum, the low frequency impedance modulus was improved three orders of magnitude, reaching $10^7\ \Omega\,cm^2$. The polarization curve showed that the I_{corr} was decreased more than three orders of magnitude, reaching $7.8 \times 10^{-9}\ A\,cm^{-2}$. The immersion test in 3.5 wt% NaCl solution showed that the long-term corrosion resistance of the composite coating could reach 50 days. This study provided a new coating for corrosion prevention of aluminum alloy. The successful preparation of composite coating on aluminum alloy surface had an extremely vital significance for improving the properties of aluminum and prolonging the service life of it in marine environment and these nanocomposites can be give other applications.

Acknowledgement

This work was sponsored by National Nature Science Foundation of China (51572248, U1806223 and 51508484).

References

[1] (a) D.A. Leal, I.C. Riegel-Vidotti, M.G.S. Ferreira, C.E.B. Marino, Corros. Sci. 130 (2018) 56;
(b) F. Yu, L. Camilli, T. Wang, D.M.A. Mackenzie, M. Curioni, R. Akid, P. Bøggild, Carbon 132 (2018) 78;
(c) M. Dong, C. Wang, H. Liu, et al., Macromol. Mater. Eng. (2019), https://doi.org/10.1002/mame.201900010 in press.
[2] (a) M. Zhang, Zhao, J. Zhang, et al., J. Polym. Res. 25 (2018) 130;
(b) M. Dong, Q. Li, H. Liu, et al., Polymer 158 (2018) 381–390.
[3] A.F. Carreira, A.M. Pereira, E.P. Vaz, A.M. Cabral, T. Ghidini, L. Pigliaru, T. Rohr, J. Coat. Technol. Res. 14 (2017) 879.
[4] F. Yu, R. Akid, Prog. Org. Coating 102 (2017) 120.
[5] (a) X. Guo, S. Ge, J. Wang, et al., Polymer 143 (2018) 155;
(b) Y. Xu, J. Qu, Y. Shen, W. Feng, RSC Adv. 8 (2018) 15181.
[6] (a) J. Liu, L. Hua, S. Li, M. Yu, Appl. Surf. Sci. 327 (2015) 241;
(b) J. Li, S. Ge, J. Wang, et al., Colloid. Surf. Physicochem. Eng. Asp. 537 (2018) 334;
(c) Y. Feng, S. Ge, J. Li, et al., Green Chem. Lett. Rev. 10 (4) (2017) 455.
[7] (a) C. Glover, C. Richards, J. Baker, G. Williams, H. McMurray, Corros. Sci. 114 (2017) 169;
(b) E. Saei, B. Ramezanzadeh, R. Amini, M. Kalajahi, Corros. Sci. 127 (2017) 186.
[8] A. Nautiyal, M. Qiao, T. Ren, T. Huang, X. Zhang, J. Cook, M. Bozack, R. Farag, Eng. Sci. 4 (2019) 70 www.doi.org/10.30919/es8d776.
[9] G.E. Luckachan, V. Mittal, Cellulose 22 (2015) 3275.
[10] A.U. Chaudhry, V. Mittal, B. Mishra, Prog. Org. Coating 110 (2017) 97.
[11] R.V. Dennis, L.T. Viyannalage, J.P. Aldinger, T.K. Rout, S. Banerjee, Ind. Eng. Chem. Res. 53 (2014) 18873.
[12] Y. Zuo, Int. J. Electrochem. Sci. 12 (12) (2017) 11728–11741.
[13] M. Mahmoudian, Y. Alias, W. Basirun, M. Ebadi, Appl. Surf. Sci. 268 (2013) 302.
[14] T. Niratiwongkorn, G.E. Luckachan, V. Mittal, RSC Adv. 6 (2016) 43237.

[15] (a) X. Zhang, Y. Zhou, J. Zhang, Prog. Nat. Sci. 27 (2017) 326;
(b) M.Y. Dong, Q. Li, H. Liu, et al., Polymer 158 (2018) 381;
(c) N. Theophile, H.K. Jeong, Chem. Phys. Lett. 669 (2017) 125.

[16] (a) Z. Zhao, P. Bai, L. Li, J. Li, L. Wu, P. Huo, L. Tan, Materials 12 (2) (2019) 330;
(b) Z. Zhao, J. Li, P. Bai, et al., Metals 9 (2) (2019) 267;
(c) Y. Zhao, B. Zhang, H. Hou, W. Chen, M. Wang, J. Mater. Sci. Technol. 35 (2019) 1044;
(d) Y. Zhao, L. Qi, Y. Jin, K. Wang, J. Tian, P. Han, J. Alloy. Comp. 647 (2015) 1104;
(e) Y. Zhao, X. Tian, B. Zhao, et al., Sci. Adv. Mater. 10 (2018) 1793–1804;
(f) Z. Zhao, P. Bai, R. Misra, et al., J. Alloys Compounds (2019), https://doi.org/10.1016/j.jallcom.2019.04.007 in press.

[17] (a) X. Cui, G. Zhu, Y. Pan, et al., Polymer 138 (2018) 203–210;
(b) H. Du, Y. An, Y. Wei, et al., Sci. Adv. Mater. 10 (2018) 1063–1072;
(c) Y. Zhang, M. Zhao, J. Zhang, et al., J. Polym. Res. 25 (2018) 130;
(d) Q. Chen, Q. Yin, A. Dong, et al., Polymer 169 (2019) 255–262.

[18] (a) L. Ma, Y. Zhu, M. Wang, X. Yang, G. Song, Y. Huang, Compos. Sci. Technol. 170 (2019) 148–156;
(b) X. Luo, J. Zhong, Q. Zhou, S. Du, S. Yuan, Y. Liu, ACS Appl. Mater. Interfaces 10 (2018) 18400;
(c) L. Ma, N. Li, G. Wu, G. Song, X. Li, P. Han, G. Wang, Y. Huang, Appl. Surf. Sci. 433 (2018) 560–567.

[19] S. Kashyap, S.K. Pratihar, S.K. Behera, J. Alloy. Comp. 684 (2016) 254.

[20] (a) H. Jang, J. Kim, H. Kang, D. Bae, H. Chang, H. Choi, Appl. Surf. Sci. 407 (2017) 1;
(b) E.B. Caldona, A.C.C. de Leon, J.D. Mangadlao, K.J.A. Lim, B.B. Pajarito, R.C. Advincula, React. Funct. Polym. 123 (2018) 10.

[21] (a) B. Kirubasankar, V. Murugadoss, J. Lin, et al., Nanoscale 10 (2018) 20414–20425;
(b) X. Li, W. Zhao, R. Yin, X. Huang, L. Qian, Eng. Sci. 3 (2018) 89–95 www.doi.org/10.30919/es8d743;
(c) J. Zhang, Z. Zhang, Y. Jiao, H. Yang, Y. Li, J. Zhang, P. Gao, J. Power Sources 419 (2019) 99–105;
(d) W. Du, X. Wang, J. Zhan, et al., Electrochim. Acta 296 (2019) 907–915;
(e) Z. Qu, M. Shi, H. Wu, Y. Liu, J. Jiang, C. Yan, J. Power Sources 410–411 (2019) 179–187;
(f) K. Le, Z. Wang, F. Wang, et al., Dalton Trans. (2019), https://doi.org/10.1039/C9DT00615J in press.

[22] (a) T. Liang, L. Qi, Z. Ma, et al., Compos. B 166 (2019) 428–435;
(b) S.V. Harb, S.H. Pulcinelli, C.V. Santilli, K.M. Knowles, P. Hammer, ACS Appl. Mater. Interfaces 8 (2016) 16339;
(c) C. Liu, Q. Fang, D. Wang, et al., ES mater, M*anufaf.* 3 (2019) 2–15 www.doi.org/10.30919/esmm5f199;
(d) J. Song, Y. Wang, J. Qiu, ES mater, M*anuaf.* 3 (2018) 29–37 www.doi.org/10.30919/esmm5f193;
(e) U. Zaheer, A. Khurram, T. Subhani, Adv. Compos. Hybrid Mater. 1 (2018) 705–721.

[23] (a) C. Hou, Z. Tai, L. Zhao, Y. Zhai, Y. Hou, Y. Fan, F. Dang, J. Wang, H. Liu, J. Mater. Chem. A 6 (2018) 9723–9736;
(b) Y. Jiao, J. Zhang, S. Liu, Y. Liang, S. Li, H. Zhou, J. Zhang, Sci. Adv. Mater. 10 (2018) 1706–1713;
(c) J. Tian, Q. Shao, X. Dong, et al., Electrochim. Acta 261 (2018) 236–245;
(d) M. Idrees, S. Batool, Q. Zhuang, J. Kong, I. Seok, J. Zhang, H. Liu, V. Murugadoss, Q. Gao, Z. Guo, Achieving carbon-rich silicon-containing ceramic anode for advanced lithium ion battery, Ceram. Int. 45 (2019) 10572–10580 in press.

[24] (a) M. Liu, Z. Yang, H. Sun, C. Lai, X. Zhao, H. Peng, T. Liu, Nano Res 9 (2016) 3735–3746;
(b) M. Liu, B. Li, H. Zhou, C. Chen, Y. Liu, T. Liu, Chem. Commun. 53 (2017) 2810–2813;
(c) M. Liu, Y. Liu, Y. Yan, F. Wang, J. Liu, T. Liu, Chem. Commun. 53 (2017) 9097–9100;
(d) W. Deng, T. Kang, H. Liu, et al., Sci. Adv. Mater. 10 (2018) 937–949.

[25] (a) W. Xie, X. Zhu, S. Yi, J. Kuang, H. Cheng, W. Tang, Y. Deng, Mater. Design 90 (1) (2016) 38–46;
(b) Y. He, Q. Chen, S. Yang, C. Lu, M. Feng, Y. Jiang, G. Cao, J. Zhang, C. Liu, Compos. A 108 (2018) 12–22;
(c) R. Ma, Y. Wang, H. Qi, et al., Compos. B 167 (2019) 396–405;
(d) X. Gong, Y. Liu, Y. Wang, et al., Polymer 168 (2019) 131–137;
(e) W. Xie, H. Cheng, Z. Chu, Z. Chen, C. Long, Ceram. Int. 37 (6) (2011) 1947;
(f) C. Wang, M. Zhao, J. Li, J. Yu, et al., Polymer 131 (2017) 263–271;
(g) W. Xie, H. Cheng, J. Kuang, Z. Chen, Z. Chu, J. Inorg. Mater. 26 (9) (2011) 939–943.

[26] (a) Y. Zhuang, F. Yu, H. Chen, J. Zheng, J. Ma, J. Chen, J. Mater. Chem. A 4 (2016) 10885;
(b) G. Huang, Z. Chen, M. Li, B. Yang, M. Xin, S. Li, Z. Yin, Acta Chim. Sin. 74 (2016) 789;
(c) Z. Yu, H. Di, Y. Ma, L. Lv, Y. Pan, C. Zhang, Y. He, Appl. Surf. Sci. 351 (2015) 986.

[27] M. Hajian, M. Reisi, G. Koohmareh, A.R. Zanjani Jam, J. Polym. Res. 19 (2012).

[28] W. Lin, Y. Sun, J. Zheng, Y. Zheng, L. Yan, B. Jiang, W. Yang, H. Chen, X. Zhang, Coatings 8 (2018) 57.

[29] C. Liu, S. Qiu, P. Du, H. Zhao, L. Wang, Nanoscale 10 (2018) 8115.

[30] D.-C. Jeong, A. Javid, L. Wen, E.J. Choi, et al., Polymer 92 (2016) 133.

[31] S. Nagappan, D.B. Lee, D.J. Seo, et al., J. Ind. Eng. Chem. 22 (2015) 288.

[32] M. Cegłowski, G. Schroeder, Chem. Eng. J. 259 (2015) 885.

[33] I.O. Arukalam, E.E. Oguzie, Y. Li, J. Colloid Interface Sci. 512 (2018) 674.

[34] Z. Yuan, J. Bin, X. Wang, M. Wang, et al., Surf. Coating. Technol. 254 (2014) 97.

[35] L. Li, J. He, J. Lei, W. Xu, et al., Surf. Coating. Technol. 279 (2015) 72.

[36] X. Cui, G. Zhu, Y. Pan, Q. Shao, et al., Polymer 138 (2018) 203.

[37] S. Liu, L. Gu, H. Zhao, J. Chen, H. Yu, J. Mater. Sci. Technol. 32 (2016) 425.

[38] M. Abd El-Fattah, A.M.A. Hasan, M. Keshawy, A.M. El Saeed, O.M. Aboelenien, Carbohydr. Polym. 183 (2018) 311.

[39] R. Torrico, S.V. Harb, A. Trentin, M.C. Uvida, S.H. Pulcinelli, C.V. Santilli, P. Hammer, J. Colloid Interface Sci. 513 (2018) 617.

[40] Y. Cao, D. Zheng, X. Li, J. Lin, C. Wang, S. Dong, C. Lin, ACS Appl. Mater. Interfaces 10 (2018) 15150.

[41] Y. Ren, E. Babaie, S.B. Bhaduri, Prog. Org. Coating 118 (2018) 1.

[42] J. Lv, Z. Liu, J. Zhang, J. Huo, Y. Yu, Polymer 121 (2017) 286.

[43] S. Krishnan, H. Arumugam, C. Kuppan, A. Goswami, M. Chavali, A. Muthukaruppan, Mater. Corros. 68 (2017) 1343.